Open access • Journal Article • DOI:10.1109/TITB.2009.2033054

Characterization of On-Body Communication Channel and Energy Efficient Topology Design for Wireless Body Area Networks — Source link

E. Reusens, Wout Joseph, Benoît Latré, Bart Braem ...+5 more authors

Institutions: Ghent University, University of Antwerp

Published on: 01 Nov 2009 - International Conference of the IEEE Engineering in Medicine and Biology Society

Topics: Path loss, Delay spread, Network topology, Wireless sensor network and Antenna (radio)

Characterization of on-body communication channel and energy efficient topology design for wireless body area networks

Characterization of On-Body Communication Channel and Energy Efficient Topology Design for Wireless Body Area Networks

Elisabeth Reusens[†], Wout Joseph[†], *Member, IEEE*, Benoît Latré[†],
Bart Braem[‡], Günter Vermeeren[†], Luc Martens[†], *Member, IEEE*,
Ingrid Moerman[†], *Member, IEEE*, and Chris Blondia[‡], *Member, IEEE*
[†] Ghent University / IBBT, Dept. of Information Technology,
Gaston Crommenlaan 8 box 201, B-9050 Ghent, Belgium
E-mail: Wout.Joseph@intec.UGent.be
[‡] University of Antwerp / IBBT, Dept. of Mathematics and Computer Science,
Middelheimlaan 1, B-2020, Antwerp, Belgium
E-mail: Bart.Braem@ua.ac.be

Abstract

Wireless Body Area Networks (WBAN) offer many promising new applications in the area of remote health monitoring. An important element in the development of a WBAN is the characterization of the physical layer of the network, including an estimation of the delay spread and the path loss between two nodes on the body. This paper discusses the propagation channel between two half-wavelength dipoles at 2.45 GHz, placed near a human body and presents an application for cross-layer design in order to optimize the energy consumption of different topologies. Propagation measurements are performed on real humans in a multipath environment, considering different parts of the body separately. In addition, path loss has been numerically investigated with an anatomically correct model of the human body in free space using a 3D electromagnetic solver. Path loss parameters and time domain channel characteristics are extracted from the measurement and simulation data. A semi-empirical path loss model is presented for an antenna height above the body of 5 mm and antenna separations from 5 cm up to 40 cm. A time domain analysis

is performed and models are presented for the mean excess delay and the delay spread. As a cross-layer application, the proposed path loss models are used to evaluate the energy efficiency of single-hop and multi-hop network topologies.

Index Terms

Propagation channel, human body, wireless body area network (WBAN), path loss, delay spread, dipole antenna, cross-layer design, energy consumption, single-hop, multi-hop, topology design.

I. Introduction

A Wireless Body Area Network (WBAN) connects independent nodes (e.g. sensors and actuators) that are situated in the clothes, on the body or under the skin of a person. The network typically extends over the whole human body and the nodes are connected through a wireless communication channel. According to the implementation, these nodes are placed in a star or multi-hop topology [1]. A WBAN offers many promising, new applications in home/health care, medicine, sports, multimedia, and many other areas, all of which make advantage of the unconstrained freedom of movement a WBAN offers.

The wireless connection between the devices of a WBAN can occur at different frequencies. Most published models use the ISM (Industrial, Scientific and Medical) frequency bands or UWB (Ultra Wide-band). The characterization of the physical layer of the network is an important step in the development of a WBAN, including an estimation of the delay spread and the path loss between two nodes on the body. Propagation near flat, homogeneous and layered phantoms has been investigated in [2], [3]. In [4], a transmission model at 2.4 GHz is proposed for different heights above a flat phantom and for different dielectric properties of the medium. Papers [5]–[11] characterize the wireless on-body channel for some specific configurations of the transmitter and receiver and provide physical-layer models. Moreover [12] and papers [13]–[19] present important research concerning the on-body wireless propagation and antennas.

This paper characterizes the physical layer in terms of path loss, delay spread, and mean excess delay for narrow band communication at 2.45 GHz between two half wavelength dipoles near a realistic human body. A total of 583 measurements are performed in a multipath environment on real humans considering different parts of the human body: arms, leg, torso, and back. In addition, the path-loss in free space has been investigated numerically using a realistic human body model. The 2.4 GHz band is selected because it is freely available and most practical existing technology for WBANs works in this band.

Based on this characterization and the physical-layer models, profound decisions can be made regarding the most optimal network architecture in terms of energy efficiency [11], [20]. They indicate that multi-hop wireless networks are required and single-hop networks are very difficult to realize. In [21], [22] the physical-layer models are used for designing and testing energy efficient and reliable cross-layer protocols, i.e. combining the MAC layer and network layer. As an application, the propagation models of this paper are used to evaluate the energy consumption of single-hop and multi-hop topologies in short range wireless networks on the human body. This is the first paper where the physical propagation analysis is used to investigate thoroughly the impact on the energy consumption on protocol level (cross-layer research) in order to determine the most optimal network topology in terms of energy efficiency. The analysis of this research can be used by manufacturers to design and validate the performance of their WBAN systems using well specified setups.

The outline of this paper is as follows. In Section II, the measurement and simulation setup and the different configurations that were investigated, are described. Section III discusses the statistical characterization of the on-body path loss in a multipath environment using measurements on real persons. The path loss in free space has been investigated on a realistic human body model using a 3D electromagnetic solver. In Section IV, a time domain analysis is executed and the mean excess delay and delay spread are studied. In Section V, the proposed path loss models are used to examine the energy performance of single-hop and multi-hop network topologies. Finally, Section VI summarizes the conclusions of this paper.

II. Measurement and Simulation Setup

A. Configuration

Two identical half-wavelength dipoles at 2.45 GHz [4], with a length of 5.7 cm and a diameter of 1 mm, are placed at various positions on the human body, which is stationary. The gain in free space of these dipoles is 2.15 dBi, and the -10 dB bandwidth of $|S_{11}|$ is about 300 MHz at 2.45 GHz if placed at a distance of 5 mm from the body. In all measurements and simulations the dipoles are placed parallel to each other and are lined up for maximal power transfer. The propagation channel characteristics depend strongly on the height of the antenna above the body [2]. In this paper we investigate the wireless channel for a separation of 5 mm between the body and the antennas. We examine the wireless on-body channel for line-of-sight narrow band communication at 2.45 GHz along the arm, the back, the torso, and the leg.

The various antenna positions on the body are shown in Fig. 1(a). Tx and Rx represent the transmitting and receiving antenna, respectively. The selection of the measurement points is made for typical WBAN sensor locations on different body parts. The next paragraphs describe the different measurement configurations along the stretched arm, the back, the torso, and the leg. The same configurations are used in the simulations.

For the measurements along the stretched arm, the transmitting antenna Tx is placed at a fixed position on the wrist and the receiving antenna Rx is moved along various positions towards the shoulder, see Fig. 1(a). In total 583 different antenna positions are investigated. The distance between the antennas varies from 5 cm up to 40 cm in steps of 1 cm. These measurements are performed on two persons: a man (height 1.73 m, weight 73 kg, BMI (body mass index) 24.4 kg/m^2) and a woman (height 1.69 m, weight 61 kg, BMI 21.4 kg/m^2), both 23 years old. A total of 214 measurements are carried out to extract the propagation statistics.

For the back and the torso, the configuration is similar. The measurements are performed on the male person lying on a table with the arms along the body. Tx is placed at approximately shoulder height at one of three different positions (left, middle, or right, see Fig. 1(a)). Rx is placed directly below Tx and is moved along a straight line in steps of 2 cm. The antenna separation varies from 5 cm up to 30 cm. A total of 132 and 102 measurements are performed on the back and the torso, respectively.

For the measurements on the leg, Tx is placed at the ankle and Rx is moved towards the knee, see Fig. 1(a). Because the surface of the leg is very different along the shin, the calf, or the side, 3 lines are taken under consideration: the front, the side and the back. The distance between the antennas varies from 5 cm up to 30 cm in steps of 2 cm. A total of 135 measurements are performed on the male person.

B. Measurement setup

The measurements are performed in a modern office. The dipoles are balanced for radiation near the human body using a λ/4-bazooka balun [23]. Fig. 1(b) shows a picture of the measurements along the arm.

A vector network analyzer (Rohde & Schwarz ZVR) is used to determine the $S_{21}(f)$-parameter (with respect to 50 Ω) between Tx and Rx for the different positions in the frequency range from 300 kHz to 4 GHz. This frequency range is necessary to be able to distinguish the direct and the reflected waves in the time domain. Here, we obtain a resolution of 0.25 ns. Time domain analysis is performed by calculating

the channel impulse responses $s_{21}(t)$ using the Inverse Fast Fourier Transform (IFFT) of the measured $S_{21}(f)$-parameters.

C. Simulation setup

The path loss along the arm and the leg is investigated by FDTD simulations in SEMCADX, using an anatomically correct model of the human body in free space (length 1.81 m, 98 kg, and BMI 29.9 kg/m^2), the NIH Visible Man model, provided by the Visible Human project of the National Library of Medicine [24], [25]. The dielectric properties of the human body tissues have been obtained from [26]. The FDTD solver SEMCADX uses a non-uniform gridding scheme. The maximum grid step in the human body model was 2 mm. The FDTD simulation domain has been determined with uniaxial perfectly matched layers with a thickness of six layers. Fig. 2 shows the simulation setup along (a) the arm and (b) the leg of the Visual Human in SEMCADX. In order to make a good comparison with the measurements, the same configurations are used in the simulations. The antenna models have equal dimensions as the λ/2-dipoles used for the measurements, and are placed 5 mm above the body. In SEMCADX, the Tx dipole is attached to an edge source. The Rx-dipole is terminated by a load of 50 Ω. The simulations were checked if steady-state was reached. Nevertheless, we have to take under consideration that the simulations are performed in a perfect free space environment, so the reflections caused by the office environment in the measurements will be absent, and that the simulation model does not fully represent the real persons in the measurements.

III. Path Loss

A. Analysis of propagation near the body

To model the path loss between the transmitting and the receiving antenna as a function of the distance, we use the following semi-empirical formula, expressed in dB and based on the Friis formula [23]:

$$P_{dB}(d) = P_{0,dB} + 10n\ log(d/d_0) = -|S_{21}|_{dB} \tag{1}$$

where the antenna separation d is expressed in cm, $P_{0,dB}$ is the path loss in dB at a reference distance d_0 (10 cm in this paper), and n [-] is the path loss exponent, which equals 2 in free space. The path loss is defined as $-|S_{21}|_{dB}$ when the generator at Tx has an input impedance of 50 Ω and Rx is terminated with 50 Ω, which allows us to regard the setup as a two-port network for which we determine S_{21}.

Since the body is within the near field of the antenna, charges on both the antenna and body surfaces interact to create a single radiating system. In this case, it is no longer possible to separate the influence of the antenna from the influence of the body. Therefore, we include the antenna as a part of the channel model throughout this analysis [27]. The values and models that are determined in this measurement campaign are specific to our particular antenna, human bodies of the 2 persons, and office environment. In the following we present the path loss models for the different human body parts that were investigated.

B. Path loss model: measurements

1) Body parts:

Fig. 3 shows the measured path loss versus Tx-Rx separation along the arm (a), the leg (b), the back (c) and the torso (d). The markers indicate the individual measurements, while the lines represent the path loss models obtained through fitting of the measurement data. Fig. 4 shows the fitted path loss models for all investigated body parts. Table I lists the parameter values of the fitted path loss models according to equation (1), and the variations of the measurement results around the model.

The path loss increases with antenna separation as expected (Figs. 3 and 4). The path loss along the arm and the leg are very similar, see Table I and Fig. 4. The reference path loss and the path loss exponent of both models are almost the same: $P_{0,dB} \approx 32.4$ dB and $n \approx 3.4$. For the measured path loss along the leg, we observe a slightly higher variation around the path loss model (standard deviation $\sigma = 5.3$ dB) compared with the measurements along the arm ($\sigma = 4.1$ dB). This is because the measurements along the leg were performed on three different lines (front, side, and back), while along the arm only one line was investigated.

The path loss model of (1) assumes that the coupling between Tx and Rx antenna is neglected for short seperations between the antennas. For a seperation of down to 5 cm the coupling between the antennas close to the body is still acceptable as no clear deviation between model and measurements is observed in Fig. 3, 4, and 5.

The path loss along the torso follows the same course as the path loss along the arm, but the path loss along the torso is the highest of the investigated body parts. This is probably due to the higher absorption in the larger volume of the trunk, and because the surface of the trunk is less flat than the surfaces of the other investigated body parts. The path loss exponent of the model along the torso is almost the same as along the arm and leg ($n \approx 3.3$). For the measured path loss along the torso, we observe a high variation

around the path loss model ($\sigma = 6.1$ dB), because the measurements along the torso were performed on three different lines: left, middle, and right. The reference path loss $P_{0,dB}$ and the path loss exponent n obtained in this paper for the model along the torso, are consistent with previous results: in [28], a path loss exponent of $n = 3.1$ and a path loss value of $P_{0,dB} = 44.6$ dB at a reference distance $d_0 = 10$ cm were measured in a large empty room for waves traveling along the front of the torso.

The path loss along the back follows a different course than the other three models. The path loss exponent is much lower ($n \approx 2.18$). This is because the surface of the back is more flat than the surface of the torso. When we take a closer look at Fig. 3(c), we can see that the path loss along the back is suddenly higher for separations between 17 cm and 23 cm, and again lower in the last part of the graph. This phenomenon is a consequence of the curvature of the spine. At waist height, the receiver will be slightly below the direct line-of-sight (LOS) path from the transmitter placed at shoulder height, which results in a higher loss. When the separation increases, the receiver comes again in a LOS situation and the path loss decreases slightly. We also see that the variation around the path loss model is relatively high ($\sigma = 5.6$ dB). This is because the measurements along the back were performed on three different lines: left, middle, and right.

The disparity in tissue compositions and in tissue thicknesses are another explanation for the variation between the path loss models for the different body parts. Due to different tissue compositions and thicknesses, the absorption in the specific body parts will vary, and thus the path loss along the body parts will differ.

2) Whole body:

Instead of investigating the different parts of the body separately, we can also define an average path loss model for the whole human body. For this purpose we consider a path loss model obtained through fitting of all measurement data. Fig. 4 shows the path loss models for the investigated body parts and for the measurements all together (full line). This curve lies between the previously derived path loss models. The parameter values of this model are also shown in Table I. The model is valid for line-of-sight communication, for the specified ranges 5 to 40 cm (Section II-A), and the investigated body parts (torso, back, arm, leg). Moreover the models are valid for the investigated subjects and the simulation model.

C. Path loss model: simulations

The path loss along the arm and the leg are numerically investigated using SEMCADX. Fig. 5 shows the path loss values and the fitted models versus Tx-Rx separation for the measurements and simulations along (a) the arm and (b) the leg. The parameter values of the fitted simulation models according to formula (1) are the following (for a reference distance d_0 = 10 cm), along the arm: $P_{0,dB}$ = 32.6 dB, n = 3.39, and the variation σ of the simulation results around the model equals 0.7 dB, and along the leg: $P_{0,dB}$ = 33.6 dB, n = 3.70, and σ = 2.7 dB.

In Figs. 5(a) and 5(b), the simulated path loss values (squares) are all situated within the set of measurements (crosses). Also, the parameters of the fitted path loss models derived from the simulations and the models obtained from the measurements (see columns for arm and leg in Table I) show good agreement, despite differences in the configurations for the human body, the environment, and the positioning of the antennas.

D. Cumulative distribution function

The model in equation (1) only represents the mean path loss [29]. In practice, there will be variations with respect to the nominal value. This variation is taken into account in the propagation model used in Section V-B.

Fig. 6 shows the cumulative distribution function (CDF) of the deviation between the measured path loss and the model along the arm. This CDF is obtained using the measurement data described in Section II-A. For the measurements along the other body parts, similar results are obtained. It was shown in [30] that the variation around the mean path loss is well described by a lognormal distribution (see lognormal fit in Fig. 6).

The mean values μ and the standard deviations σ of the lognormal distributions for the different body parts, fitted using a least-square error method, are provided in Table II. The values of these CDF parameters indicate that the path loss models show very good correspondence with the measurement results. The mean values of the fitted CDFs of the deviation is close to 0 dB and the standard deviations differ less than 1 dB from the standard deviation of the measured values (0.7 dB, 0.6 dB, 0.4 dB, and 0.6 dB difference for arm, leg, back, and torso, respectively). Moreover, the different data sets also passed a Kolmogorov-Smirnov (K-S) test for normality at significance level 5 $\%$, indicating that the deviation of measured path loss and model (in dB) is normally distributed [31].

IV. Delay Spread

A. Definitions

Time domain analysis is performed by calculating the channel impulse responses $h(t) = s_{21}(t)$ using the Inverse Fast Fourier Transform (IFFT) of the measured frequency transfer functions $S_{21}(f)$ from 300 kHz to 4 GHz. Fig. 7 shows the normalized impulse response from 0 ns to 40 ns for a measurement along the arm for an antenna separation of 5 cm, on a logarithmic scale. It can be seen that most energy is received via the direct path with different multipath reflections after some time.

Power delay profiles (PDP) were calculated for all the measurement positions. For the following analysis only peaks (see Fig. 7) of less than 35 dB below the maximum value of the PDP are taken under consideration. The points in time where the peaks in the PDP occur, are indicated by τ_i with i = 1, 2, ..., N, where N is the number of peaks taken under consideration varying for each measurement. The PDP is characterized by the first central moment (mean excess delay τ_0), and the square root of the second moment (RMS delay spread τ_{rms}). The RMS delay spread is a measure of multipath spread within the channel, an important parameter for characterizing time dispersion or frequency selectivity, and provides a figure of merit for estimating data rates for multipath channels [29]. The delay spread τ_{rms} and mean excess delay τ_0 are defined in [10], [29].

B. Delay spread model

Figs. 8(a) and 9(a) show the mean excess delay τ_0 and the RMS delay spread τ_{rms} versus antenna separation along the arm. For the measurements along the other body parts, similar results are obtained.

The values of τ_0 and τ_{rms} increase with antenna separation. The mean excess delay τ_0 follows a linear course as a function of the antenna separation and is modeled as follows [8]:

$$\tau_0(d) = A \cdot d + B \quad [ns] \tag{2}$$

with the distance d between Tx and Rx in cm and A [ns/cm] and B [ns] the parameters of the model. Fig. 8(b) shows the fitted τ_0 models, derived from the measurements, using a least-square error method.

The course of the RMS delay spread τ_{rms} versus antenna separation is divided into two parts with a breakpoint d_{bp}. The first part is modeled by an exponential fit and the second part by a logarithmic fit,

with the following equations:

$$\tau_{rms}(d) = C(e^{D \cdot d} - 1) \quad [ns] \qquad for\ d \leq d_{bp} \tag{3}$$

$$= E + F\ ln(d/d_{bp}) \quad [ns] \quad for\ d > d_{bp} \tag{4}$$

with the breakpoint d_{bp} and the distance d between Tx and Rx in cm and C [ns], D [1/cm], E [ns] and F [ns] the parameters of the model. Fig. 9(b) shows the fitted τ_{rms} models, derived from the measurements, using a least-square error method.

The parameter values of the fits and the variations of the measurement results around the model, are shown in Table III. The τ_0 models along the back and along the torso are very similar. Also along the arm and the leg, the difference between the τ_0 models is small. The lowest values occur along the arm and the leg, because the limbs have a much smaller volume and surface, which results in less multipath reflections. As a consequence, the τ_{rms} values are the lowest along the arm and the highest along the torso.

C. Cumulative distribution function

In this section we verify whether τ_0 and τ_{rms} follow a lognormal distribution. Other different empirical distributions were applied, however, lognormal proved to be the best fit. We investigate the deviation of the measured values and the models, see equations (2)-(4). The mean values and the standard deviations of the fits of the CDFs for all measurements, fitted using a least-square error method, are provided in Table II. These parameters indicate that both models show very good correspondence with the measurement results. The mean values are close to 0 dB and the standard deviations differ less than 1 dB from the variation of the measured values discussed in Section IV-B. Moreover, the different data sets along each body part separately also passed a Kolmogorov-Smirnov (K-S) test for normality at significance level 5 $\%$, indicating that the deviation of the measured values of τ_0 and τ_{rms} and the models (in dB) is normally distributed [31].

V. Impact on Energy Efficient Network Topology

A. Background

The radios that are used in WBANs are very small, which leaves only limited space for a battery while recharging is not always possible. Furthermore, an important requirement for WBANs is a large lifetime

of the network (e.g. implanted devices should last for at least a year). Therefore, energy efficiency is of uttermost importance in order to increase the lifetime of the network and to meet the requirements.

Regular ad-hoc and sensor networks mostly use multi-hop communication where nodes in the network act as routers for other nodes to help guarantee connectivity. Current implementations in a WBAN, however, assume single-hop communication where all information is sent directly to the receiver. The work of Zasowski [11] was a first attempt to justify the use of multi-hop in a WBAN, where intermediate hops are used for reaching the receiver. They use an energy model that is only applicable to UWB communication and conclude that the criteria whether to use a multi-hop strategy depend on the ratio of the energy consumption needed for decoding/coding and receiving/generating a UWB-pulse. In [32] reliability is experimentally investigated by measuring the packet delivery ratio without imposing a MAC-protocol. A multi-hop strategy turns out the most reliable.

In this section, we evaluate the energy consumption for narrowband communication at 2.4 GHz based on a commercial available radio. First, a propagation model and an appropriate energy model are selected. Then, this energy model is subsequently used for analyzing the energy consumption. The goal is to investigate which topology is the most energy efficient in WBANs: single-hop or multi-hop communication. A preliminary study has been done in [22] where only a line topology and binary tree was considered.

B. Selection of Propagation and Energy Model

When determining an energy model of the radio, it is important to notice that the channel model derived in the previous section only accounts for line of sight (LOS) propagation and does not consider, for example, the communication between the back and torso nor does it take into account the curvature effects of the body. In [33], the path loss is modeled in non-line of sight (NLOS) situations around the torso for UWB-communication in a band of 3 to 6 GHz. This model can be used for a narrowband system around 2.4 GHz as it is relatively close to the band of 3 GHz. Further, their definition of the path loss is the same as ours. We selected this model because it is the best NLOS model available and moreover the path loss exponents and model parameters correspond well with the ones of our model for LOS. Both models use (1), but with different parameters. For the LOS propagation, the parameters can be found in Table I (we use the whole body model). The NLOS propagation has the following parameter values: d_0 = 10 cm, $P_{0,dB}$ = 48.8 dB, n = 5.9, and σ = 5.0 dB [33]. It can be remarked that a higher path loss and a higher path loss exponent along the NLOS channel than along the LOS channel is observed due to

diffraction around the human body and absorption of a large amount of radiation by the body.

The model in (1) only represents the mean path loss [29]. We also have to take the variations with respect to the nominal value into consideration. Therefore, a variation component (see Section III-D) is included in propagation model. It is crucial to account for this, in order to provide a certain reliability of communications. The received signal strength $p^j_{r,dB}$ at a node j from a node i sending with transmitting power $p^i_{s,dB}$ over a distance $d_{i,j}$ between the nodes, can be written as

$$p^j_{r,dB}(d_{i,j}) \;=\; p^i_{s,dB} \;-\; P_{dB}(d_{i,j}) \;-\; X_{\sigma,dB} \quad [dBW] \tag{5}$$

where P_{dB} is the value predicted by the path loss model in equation (1) and the variation component $X_{\sigma,dB}$ is a zero-mean Gaussian random variable with standard deviation σ (specified by the path loss model). The condition for communication is that $p^j_{r,dB}$ is higher than a certain threshold p_{th} at the receiver. As a result, the probability $Con(i,j)$ that two nodes i and j are connected can be formulated as:

$$\begin{aligned} Con(i,j) &= \Pr\left[p^j_{r,dB}(d_{i,j}) > p_{th}\right] && (6)\\ &= \Pr\left[X_{\sigma,dB} - p^i_{s,dB} + P_{dB}(d_{i,j}) + p_{th} < 0\right] && (7)\\ &= \frac{1}{2} - \frac{1}{2}\,\mathrm{erf}\left(\frac{-p^i_{s,dB} + P_{dB}(d_{i,j}) + p_{th}}{\sqrt{2\pi}\sigma}\right) && (8) \end{aligned}$$

If a reliable WBAN is desired, for example, a connection probability $Con(i,j)$ of 99% can be demanded.

An important element in analyzing the energy efficiency of a network, is to have a good energy model of the radio at one's disposal. As we are only interested in the energy consumption of the communication, which is much larger than the energy used for sensing [34], we ignore the latter in this paper. Different energy models can be found in the literature. We have adapted the first-order model described in [35]. This model assumes a d^2 energy loss due to channel transmission with d the distance between Tx and Rx. Here, we transform the model in a more general one by changing d^2 to d^n, where n represents the path loss coefficient (n = 3.11 for the LOS channel and n = 5.9 for the NLOS channel). Doing so, the energy model becomes the following:

$$E_{tx}(k,d,n) = E_{TXelec} \cdot k \;+\; E_{amp}(n) \cdot k \cdot d^n \quad [J] \tag{9}$$

$$E_{rx}(k) = E_{RXelec} \cdot k \quad [J] \tag{10}$$

In these formulas, E_{tx} [J] represents the transmission energy, E_{rx} [J] the receiver energy, E_{TXelec} [nJ/bit] and E_{RXelec} [nJ/bit] the energy dissipated by the radio to run the circuitry for the transmitter and receiver

respectively, $E_{amp}(n)$ [J/(bit $\cdot$ m^n)] the energy for the transmit amplifier, and k [bit] the number of bits sent. The radios are presumed to have power control and consume the minimal energy needed to reach the receiver. The specific values of these parameters are hardware dependent. We have determined these parameters for two commercially available transceivers which are frequently used in sensor networks: the Nordic nRF2401 low power single chip transceiver [36] and the Chipcon CC2420 transceiver [37] used in Telos-B motes. Both transceivers work in the 2.4–2.4835 GHz band and have a very low power consumption. The appropriate values for the parameters above were obtained by fitting equations (9) and (10) to the actual power consumption of the devices which can be found in the datasheets. The distance used in equation (9) is the maximal distance that can be reached between Tx and Rx. If the receiver is positioned a little bit further, it is no longer within the receive range of the sender and the received signal is below the sensitivity of the radio. This maximal distance is calculated for each output power level (p_{tx}) using equations (1) and (5) and the assumption that the maximal path loss (P_{dB}) equals the difference between the sensitivity of the radio and p_{tx}. A reliability of 99% is assumed. Table IV shows the results for both radios for the different values of the path loss exponent n for the LOS and the NLOS channel. It can be seen that the Nordic radio has a lower energy consumption per bit. This can be explained by the higher bitrate that can be obtained by the Nordic transceiver. Hence, we will use the parameters of the Nordic radios in our further calculations.

C. Studied scenario

In this paper, it is not our intention to develop a routing protocol for a WBAN. We merely want to show that a multi-hop approach is inevitable in a WBAN when evaluating the energy efficiency. Therefor, we consider a regular tree network as it allows a more generic way of approaching the problem. More specifically, we assume a ζ-balanced tree, i.e. a tree where all the children have exactly ζ children. In Fig. 10, a balanced tree with ζ = 2 is depicted. There are L levels in the network that are numbered consecutively from level 1 for the nodes that are the furthest away from the sink up to level L for the nodes closest to the sink. We assume that the distance between the levels is fixed at an inter-node distance d_{in}. The spacing between the nodes is uniform in order to make the analysis more general. If a scenario was used with predetermined test locations of the nodes on the body, the results would only be applicable to that specific scenario. Indeed, it would be interesting to see how this scenario would behave, but this information can also be derived from our more general analysis with uniform spacing. As mentioned in

Section V-B, we distinguish between LOS and NLOS communication. The links between neighboring nodes is modeled as a LOS situation. In other situations, the path loss for NLOS is used. By using both LOS and NLOS, communication from one side of the body to the opposite is considered. Further, by changing the distance d_{in}, communication between a leg or arm can be modeled.

We assume that all nodes in the tree network generate packets at the same rate, so during each duty cycle each node wants to send one packet to the sink. Moreover, a perfect duty cycle is assumed, i.e. a sensor only turns on its radio when it sends or receives data. The main purpose of this approach is to orthogonalize the results from this study and the properties of specific MAC-protocols.

As the energy efficiency is considered as one of the most important performance issues of WBANs, we use the network lifetime as metric, which we define as the time for the first node to die. In order to have a high network lifetime, the most consuming node should be made more energy efficient. This metric forces us to consider all nodes to be equally important, which corresponds to the fact that a WBAN has no redundant nodes.

We will try to improve the energy performance for this topology. In a first instance, we use a very simple type of multi-hop routing where the data is sent to the nearest neighbor. In a second instance, the multi-hop routing is made more complex by adding relay devices and by letting the nodes cooperate.

D. Single-hop versus Multi-hop

In the tree network of Fig. 10, the energy usage per bit for a node at level y when using single-hop (E_{SH}) can be written as:

$$E_{SH}(y, d_{in}) = \ E_{TXelec} \ + E_{amp}(n) \ ((L - y + 1) \cdot d_{in})^n \ \ [J/bit] \tag{11}$$

Whereas the energy usage for a node at level y in a multi-hop network (E_{MH}) with the tree topology of Fig. 10 is given by:

$$E_{MH}(y, d_{in}) \ = \ \zeta \cdot \sum_{i=0}^{y-2} \zeta^i \cdot E_{RXelec} \cdot k + \sum_{i=0}^{y-1} \zeta^i \cdot k \cdot (E_{TXelec} \ + \ E_{amp}(\eta) \cdot d_{in}^{\eta}) \ \ [J/bit] \tag{12}$$

Due to the ζ-balanced tree, each node has ζ children, what explains the factor ζ at the receiver part.

Fig. 11 shows the energy usage ratio E_{MH}/E_{SH} [-] of multi-hop versus single-hop scenario, in a tree network for ζ = 2 with 4, 5 or 6 levels and d_{in} = 20 cm or 30 cm. If $E_{MH}/E_{SH} < 1$, then multi-hop is better and if $E_{MH}/E_{SH} > 1$, then single-hop is better.

The results show that the nodes closest to the sink (at level 6) perform really bad when using multi-hop: they become *hotspots* using more than 100 times the energy of the single-hop scenario because they are relaying a lot of data from the nodes at the other levels. However, far away from the sink, at level 1 in Fig. 11, the single-hop scenario performs up to 1000 times worse than the multi-hop scenario because of the much higher path loss. It is clear that distance plays an important role in these results. When the distance between the nodes increases, the high path loss in the single-hop scenario has a dramatical impact on the performance, resulting in a higher energy usage.

E. Improving the Energy Efficiency

The results obtained in the previous section are used to improve the energy efficiency of communication taking place in WBANs. The network lifetime can be improved by tackling the energy usage at the nodes consuming the most energy.

We observe that in the single-hop scenario, there is clearly room for energy saving at the nodes further away from the sink (see Fig. 11). These nodes consume the most energy and consequently will die first. However, we also see that in the multi-hop scenario more energy is consumed by the nodes closest to the sink (see Fig. 11), as they have to forward the data received from nodes further away. Based on these observations, we will consider two mechanisms that can be used in order to improve the network lifetime considerably: relaying and cooperation.

A first solution encompasses the introduction of dedicated relay devices. These are special nodes which only handle traffic relaying and do not do any sensing themselves, thus more energy is available for communication purposes. The main idea is that proper placement of relay nodes can bridge the performance gap for the nodes far away from the sink in the case of single-hop traffic and distribute the load from the nodes closer to the sink in the case of multi-hop traffic. In this study, we assume that the relay nodes are placed next to existing nodes, so the inter-node distance d_{in} remains the same.

For a node relaying traffic from z nodes, the energy usage per bit E_R is similar to the energy usage of a regular node in a multi-hop tree network, see equation (12), minus the cost of transmitting its own packets:

$$E_R(z, d_{in}) = \ z \cdot (E_{RXelec} + (E_{TXelec} + E_{amp}(n) \cdot d_{in}^n)) \quad [J/bit] \tag{13}$$

When properly placed, relay nodes can considerably improve the lifetime of the network, as we inject

more energy in the network. However, it is not always feasible to use relay nodes. Specifically in the case of WBANs, placing more sensors on users does not really improve comfort. Hence, other methods need to be used.

Another solution to improve the network lifetime, is cooperation, i.e. the nodes cooperate in forwarding the data from one node toward the central device. When we compare the energy usage [J/bit] in a single-hop topology to the energy usage in a multi-hop topology in Fig. 12, it is obvious that there is a lot of residual energy available at higher levels, i.e. the nodes the closest to the central device. Indeed, by using this energy supply, the lifetime of the network will be bounded by the energy usage of the nodes on level 3. The data of the nodes on level 1 and 2 will be forwarded to level 4 and level 5, respectively. This will lower the energy consumption of these nodes, as was the case with the relay devices. Hence, the network lifetime can be improved without the addition of extra relay devices.

The following formula is used to calculate the number of nodes that can be relayed by the nodes at level k when the energy consumption is limited by the nodes at level l:

$$\text{\#nodes supported} = \left\lfloor \frac{E_{SH}(l, d_{in}) - E_{SH}(k, d_{in})}{E_R(1, (L - k + 1) \cdot d_{in})} \right\rfloor \tag{14}$$

with $\lfloor\ \rfloor$ representing the floor function. Using this formula, it can be calculated that, e.g., for a network with an inter-node distance d_{in} = 20 cm, the data of up to 4 nodes can be relayed by the nodes at level 4.

Fig. 12 shows an example of the results when using the cooperation approach in a tree network with ζ = 2 and d_{in} = 20 cm. The almost horizontal line of energy usage in the cooperating network demonstrates a good trade off between single-hop and multi-hop network setups, using a smart combination of both. We can also see that the energy consumption of a node at level 4 or 5 in the cooperating network (sending its own data and relaying the data of the other nodes) still remains slightly below the energy consumption of nodes at level 3. The maximal energy usage in the cooperating network (see Fig. 12) is a lot lower compared to the single-hop or multi-hop approaches, resulting in a higher network lifetime

VI. Conclusions

Transmission between two half-wavelength dipoles near the human body is studied at 2.45 GHz. Propagation measurements are performed on two real humans, considering different parts of the human body separately. In total, 583 measurements are performed, enabling a statistical approach. We characterize in this paper the path loss for different parts of the human body (arm, back, torso, and leg) obtained

by measurements on actual humans and by simulations with a realistic human body phantom. For the investigated subjects in a multipath environment and a realistic phantom in free space, the path loss exponent is about 3.1 for line-of-sight communication. Path loss along arm and leg is similar. The path loss along the torso is the highest of the investigated body parts. The path loss models obtained from the simulations show a good agreement with the models derived from the measurements, despite dissimilarities in the configurations with respect to human body and environment. The cumulative distribution functions of the deviation of measured path loss and models are well described by a lognormal distribution. The mean values and the standard deviations of the fits indicate the lognormal behaviour and show that the models agree excellently with the measurements.

The mean excess delay τ_0 and the RMS delay spread τ_{rms} are also studied. These parameters increase with antenna separation. Models are determined for τ_0 and τ_{rms} and show excellent correspondence with the measurement results. The cumulative distribution functions of the deviation of τ_0 and τ_{rms} and the derived models are well described by a lognormal distribution.

The physical propagation analysis is used to investigate thoroughly a detailed application on protocol level (cross-layer research) in order to determine the most optimal network topology in terms of energy efficiency. We showed for the considered subjects, that single-hop communication is difficult in terms of energy consumption and multi-hop communication would be a better choice. If single-hop communication does not provide satisfying results for these investigated cases, then this means that single hop will not work for all people. Doing so, we show that multi-hop communication is needed.
We have shown that using relay devices, or a more cooperative approach, can improve energy consumption largely, as this distributes the transmission load over the entire network. This study should be seen as a first step towards a highly energy efficient WBAN. Based on the results carried out from this paper, new communication protocols can be developed or existing ones can be adapted. They should be based on a smart combination of single and multi-hop networking. Metrics and algorithms should be developed that can decide which node to forward to and that allow a node to communicate whether it is capable of cooperating. The contributions of this paper should be considered a source of inspiration for WBAN protocol developers.

This analysis is performed for two subjects and a realistic heterogeneous phantom model and as there are many differences among people (age, height, figure, physical condition, ...), more future research is

needed. Movement is not taken into account in this paper. This can also be part of future research both for measurements and simulations.

VII. Acknowledgment

This research is partly funded by the Fund for Scientific Research - Flanders (FWO-V, Belgium) project G.0531.05. W. Joseph is a Post-Doctoral Fellow of the FWO-V (Research Foundation - Flanders). The authors would like to thank Toon Depessemier for helping us during the measurement campaign.

References

[1] B. Latré, G. Vermeeren, I. Moerman, L. Martens, F. Louagie, S. Donnay, and P. Demeester, "Networking and propagation issues in body area networks," in *11th Symposium on Communications and Vehicular Technology in the Benelux*, Ghent, Belgium, Nov. 2004, available on CD-ROM.

[2] L. Roelens, W. Joseph, and L. Martens, "Characterization of the path loss near flat and layered biological tissue for narrowband wireless body area networks," in *International Workshop on Wearable and Implantable Body Sensor Networks (BSN 2006)*, MIT Media Lab, Boston, USA, Apr. 2006, pp. 50–53.

[3] L. Roelens, S. Van den Bulcke, W. Joseph, G. Vermeeren, and L. Martens, "Path loss model for wireless narrowband communication above flat phantom," *IEE Electronics Letters*, vol. 42, no. 1, pp. 10–11, Jan. 2006.

[4] L. Roelens, W. Joseph, E. Reusens, G. Vermeeren, and L. Martens, "Characterization of scattering parameters near a flat phantom for wireless body area networks," *IEEE Transactions on Electromagnetic Compatibility*, vol. 50, no. 1, pp. 185–193, Feb. 2008.

[5] J. Ryckaert, P. De Doncker, R. Meys, A. de Le Hoye, and S. Donnay, "Channel model for wireless communication around human body," *IEE Electronics Letters*, vol. 40, no. 9, pp. 543–544, Apr. 2004.

[6] A. Alomainy, Y. Hao, X. Hu, C. Parini, and P. Hall, "UWB on-body radio propagation and system modelling for wireless body-centric networks," *IEE Proceedings-Communications*, vol. 153, no. 1, pp. 107–114, Feb. 2006.

[7] A. Fort, C. Desset, P. De Doncker, P. Wambacq, and L. Van Biesen, "An ultra-wideband body area propagation channel model - from statistics to implementation," *IEEE Trans. Microwave Theory and Tech.*, vol. 54, no. 4, pp. 1820–1826, Apr. 2006.

[8] E. Reusens, W. Joseph, G. Vermeeren, and L. Martens, "On-body measurements and characterization of wireless communication channel for arm and torso of human," in *International Workshop on Wearable and Implantable Body Sensor Networks (BSN 2007)*, Aachen, Germany, March 2007, pp. 264–269.

[9] E. Reusens, W. Joseph, G. Vermeeren, L. Martens, B. Latré, I. Moerman, B. Braem, and C. Blondia, "Path loss models for wireless communication channel along arm and torso: measurements and simulations," in *2007 IEEE Antennas and Propagation Society International Symposium*, Honolulu, Hawaii, June 2007, pp. 345–348.

[10] E. Reusens, W. Joseph, G. Vermeeren, D. Kurup, and L. Martens, "Real human body measurements, model, and simulations of 2.45 GHz wireless body area network communication channel," in *International Workshop on Wearable and Implantable Body Sensor Networks (BSN 2008)*, Hong Kong, China, June 2008, pp. 149–152.

[11] T. Zasowski, F. Althaus, M. Stäger, A. Wittneben, and G. Tröster, "UWB for noninvasive wireless body area networks: channel measurements and results," in *2003 IEEE Conference on Ultra Wideband Systems and Technologies*, Reston, VA, Nov. 2003, pp. 285–289.

[12] P. Hall and Y. Hao, *Antennas and Radio Propagation for Body-Centric Wireless Communications*. London, UK: Artech House, 2006.

[13] P. S. Hall, Y. Hao, Y. I. Nechayev, A. Alomainy, C. C. Constantinou, C. Parini, M. R. Kamarudin, T. Z. Salim, D. T. M. Hee, R. Dubrovka, A. S. Owadally, W. Song, A. Serra, P. Nepa, and M. Gallo, "Antennas and propagation for for on-body communication systems," *IEEE Antenna and Propagation Magazine*, vol. 49, no. 3, pp. 41–58, June 2007.

[14] S. Kovacs, G. Pedersen, P. Eggers, and K. Olesen, "Ultra wideband radio propagation in body area network scenarios," in *ISSSTA Proceedings*, 2004, pp. 102–106.

[15] A. Alomainy, Y. Hao, A. Owadally, C. Parini, Y. Nechayev, P. Hall, and C. C. Constantinou, "Statistical analysis and performance evaluation for on-body radio propagation with microstrip patch antennas," *IEEE Transactions on Antennas and Propagation*, vol. 55, no. 1, pp. 245–248, January 2007.

[16] Y. Zhao, Y. Hao, A. Alomainy, and C. G. Parini, "Uwb on-body radio channel modelling using ray theory and sub-band fdtd method," *IEEE Transactions on Microwave Theory and Techniques, Special Issue on Ultra-Wideband*, vol. 54, no. 4, pp. 1827–1835, April 2006.

[17] S. L. Cotton and W. G. Scanlon, "Statistical analysis of indoor multipath fading fo a narrowband wireless body are network," in *IEEE 17th International Symposium on Personal, Indoor and Mobile Radio Communications*, September 2006, pp. 1–5.

[18] T. Tayamachi, Q. Wang, and J. Wang, "Transmission characteristic analysis for uwb body area communications,?international symposium on electromagnetic compatibility," in *IEEE International Symposium on Electromagnetic Compatibility (EMC 2007)*, October 2007, pp. 75–78.

[19] A. F. Molisch, K. Balakrishnan, C. Chong, S. Emami, A. Fort, J. Karedal, J. Kunisch, H. Schantz, U. Schuster, and K. Siwiak, "IEEE 802.15.4a Channel Model - Final Report," IEEE 802.15.4a Channel Modeling Subgroup, Tech. Rep., 2004, online available at http://www.ieee802.org/15/pub/04/15-04-0662-02-004a-channel-model-final-report-r1.pdf.

[20] B. Braem, B. Latré, I. Moerman, C. Blondia, E. Reusens, W. Joseph, L. Martens, and P. Demeester, "The need for cooperation and relaying in short-range high path loss sensor networks," in *2007 International Conference on Sensor Technologies and Applications (SENSORCOMM 2007)*, Valencia, Spain, Oct. 2007, pp. 566–571.

[21] B. Latré, B. Braem, I. Moerman, C. Blondia, E. Reusens, W. Joseph, and P. Demeester, "A low-delay protocol for multihop wireless body area networks," in *Fourth Annual International Conference on Mobile and Ubiquitous Systems: Networking & Services (MobiQuitous 2007)*, Philadelphia, Pennsylvania, USA, Aug. 2007, pp. 1–8.

[22] B. Braem, B. Latré, C. Blondia, I. Moerman, and P. Demeester, "Improving reliability in multi-hop body sensor networks," in *The Second International Conference on Sensor Technologies and Applications (SENSORCOMM 2008)*, Cap Esterel, France, Aug. 2008.

[23] C. A. Balanis, *Antenna Theory, Analysis and Design*. New York, NY: 1st ed. Harper & Row, 1982, pp. 64-65, 365-367.

[24] National Library of Medicine. [Online]. Available: http://www.nlm.noh.gov/research/visible/visible_human.html.

[25] J. Ziriax, D. Le Blanc, P. A. Mason, and W. D. Hurt, "Finite-difference time-domain for personal computers," in *21st Ann. Meeting of the Bioelectromagnetics Soc.*, Long Beach CA, June 1999, p. 57.

[26] C. Gabriel, "Compilation of the dielectric properties of body tissues at RF and microwave frequencies," Brooks Air Force Base, San Antonio, TX, Tech. Rep. AL/OE-RE-1996-0037, 1996, [Online]. Available: http://www.fcc.gov/cgi-bin/dielec.sh.

[27] R. Vaughan and J. B. Andersen, *Channels, Propagation and Antennas for Mobile Communications*. Michael Faraday House, Stevenage, UK: Electromagnetic Waves Series 50, The Institute of Electrical Engineers (IEE), 2003.

[28] A. Fort, C. Desset, J. Ryckaert, P. De Doncker, L. Van Biesen, and P. Wambacq, "Characterization of the ultra wideband body area propagation channel," in *IEEE International Conference on Ultra-Wideband (ICU 2005)*, Zurich, Switzerland, Sept. 2005, available on CD-ROM.

[29] Saunders, *Antennas and propagation for wireless communication systems*. West Sussex, England: Wiley, 1999.

[30] A. Fort, C. Desset, J. Ryckaert, P. De Doncker, L. Van Biesen, and S. Donnay, "Ultra wide-band body area channel model," *IEEE International Conference on Communications (ICC)*, vol. 4, pp. 2840–2844, May 2005.

[31] M. H. Kutner, C. J. Nachtsheim, J. Neter, and W. Li, *Applied Linear Statistical Models, 5th ed.* Berkshire, UK: McGraw-Hill, 2005.

[32] A. Natarajan, M. Motani, B. de Silva, K.-K. Yap, and K. C. Chua, "Investigating network architectures for body sensor networks," in *HealthNet '07: Proceedings of the 1st ACM SIGMOBILE international workshop on Systems and networking support for healthcare and assisted living environments*. New York, NY, USA: ACM, 2007, pp. 19–24.

[33] A. Fort, J. Ryckaert, C. Desset, P. De Doncker, P. Wambacq, and L. Van Biesen, "Ultra-wideband channel model for communication around the human body," *IEEE Journal on Selected Areas in Communications*, vol. 24, pp. 927–933, Apr. 2006.

[34] M. Welsh, "Exposing resource tradeoffs in region-based communication abstractions for sensor networks," *SIGCOMM Computer Communication Review*, vol. 34, no. 1, pp. 119–124, Jan. 2004.

[35] W. Heinzelman, A. Chandrakasan, and H. Balakrishnan, "Energy-efficient communication protocol for wireless microsensor networks," in *Proceedings of the 33rd Annual Hawaii International Conference on System Sciences*, vol. 2, Jan. 2000.

[36] "Nordic nrf 2401 datasheet." [Online]. Available: http://www.nordicsemi.no/index.cfm?obj=product&act=display&pro=64#

[37] "Chipcon cc2420 datasheet." [Online]. Available: www.chipcon.com/files/CC2420_Brochure.pdf

LIST OF TABLES

LIST OF FIGURES

TABLE I

MEASUREMENTS: PARAMETER VALUES OF THE PATH LOSS MODELS.

parameter	**arm**	**leg**	**back**	**torso**	**whole body**
d_0 [cm]	10	10	10	10	10
$P_{0,dB}$ [dB]	32.2	32.5	36.8	41.2	35.2
n [-]	3.35	3.45	2.18	3.23	3.11
σ [dB]	4.1	5.3	5.6	6.1	6.1

TABLE II

CDF OF THE DEVIATION OF MEASURED PATH LOSS P_{dB}, MEAN EXCESS DELAY τ_0, AND RMS DELAY SPREAD τ_{rms} WITH RESPECT TO THE MODELS: LOGNORMAL DISTRIBUTION FIT.

	parameter	**arm**	**leg**	**back**	**torso**
P_{dB}	σ [dB]	3.4	5.9	5.2	5.5
	μ [dB]	-0.2	-0.3	0.0	-0.7
τ_0	σ [ns]	1.12	2.03	1.89	1.91
	μ [ns]	-0.05	0.00	-0.06	0.00
τ_{rms}	σ [ns]	0.98	2.53	1.34	1.39
	μ [ns]	-0.04	0.25	0.01	0.00

TABLE III

PARAMETER VALUES OF THE MODELS FOR THE MEAN EXCESS DELAY τ_0 AND THE RMS DELAY SPREAD τ_{rms}.

model	**parameter**	**arm**	**leg**	**back**	**torso**	**whole body**
$\tau_0(d) = A \cdot d + B$	A [ns/cm]	0.35	0.41	0.72	0.76	0.54
	B [ns]	-1.11	-1.81	-1.96	-2.71	-1.82
	σ_{τ_0} [ns]	1.14	2.65	1.93	1.97	3.70
$\tau_{rms}(d) = C \cdot (e^{D \cdot d} - 1)$	C [ns]	1.41	0.67	1.88	0.58	0.69
for $d \leq d_{bp}$	D [1/cm]	0.09	0.15	0.15	0.23	0.20
$\tau_{rms}(d) = E + F \cdot ln(d/d_{bp})$	E [ns]	9.97	6.40	13.01	12.23	8.68
for $d > d_{bp}$	F [ns]	5.88	16.72	3.03	6.13	9.11
	d_{bp} [cm]	22.3	16.2	14.0	13.2	13.3
	$\sigma_{\tau_{rms}}$ [ns]	1.06	3.18	1.36	1.44	3.07

TABLE IV

PARAMETER VALUES FOR THE NORDIC NRF2401 AND CHIPCON CC2420 TRANSCEIVERS.

parameter	**nRF2401**	**CC2420**
E_{TXelec} [nJ/bit]	16.7	96.9
E_{RXelec} [nJ/bit]	36.1	172.8
$E_{amp}(n = 3.11)$ [J/(bit $\cdot$ m^n)]	1.97e-9	2.71e-7
$E_{amp}(n = 5.9)$ [J/(bit $\cdot$ m^n)]	7.99e-6	9.18e-4

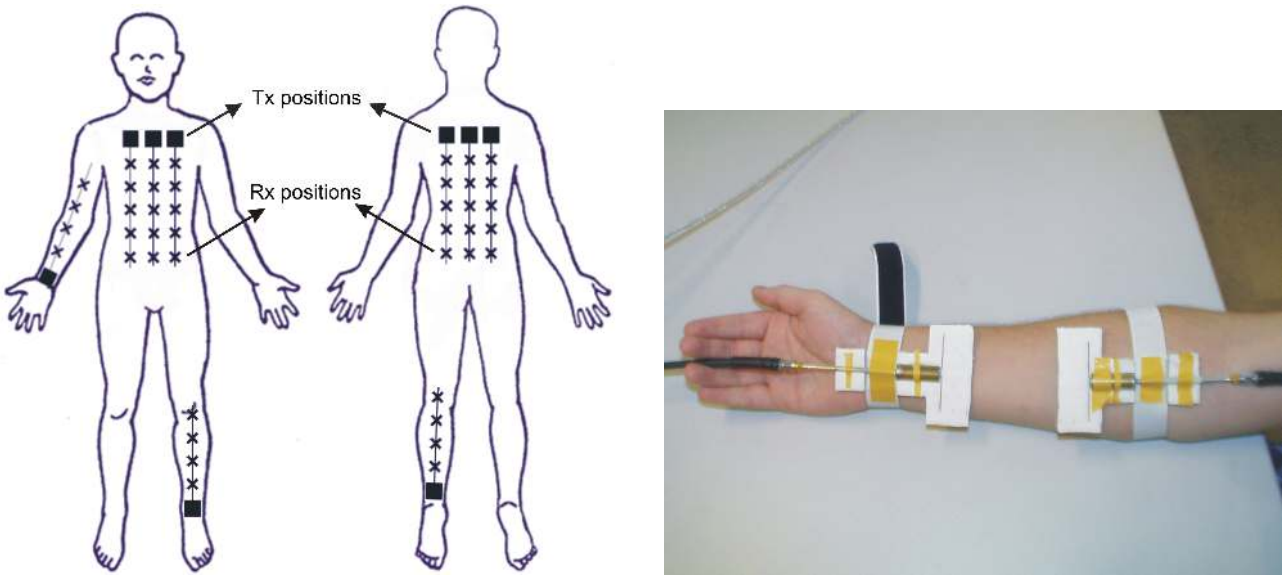

(a) (b)

Fig. 1. Measurement setup: (a) Antenna positions on the body (■ = Tx and x = Rx), (b) Measurement setup: picture of measurements on the arm.

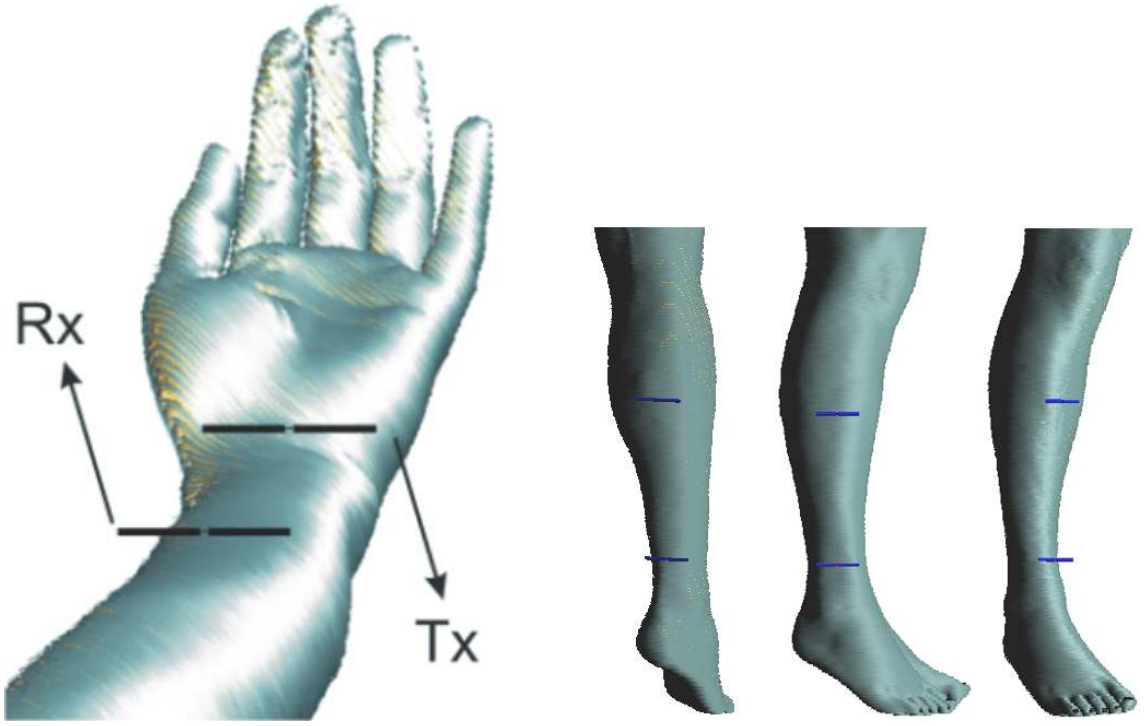

(a) (b)

Fig. 2. Simulation setup: (a) arm and (b) leg of Visual Human in SEMCADX.

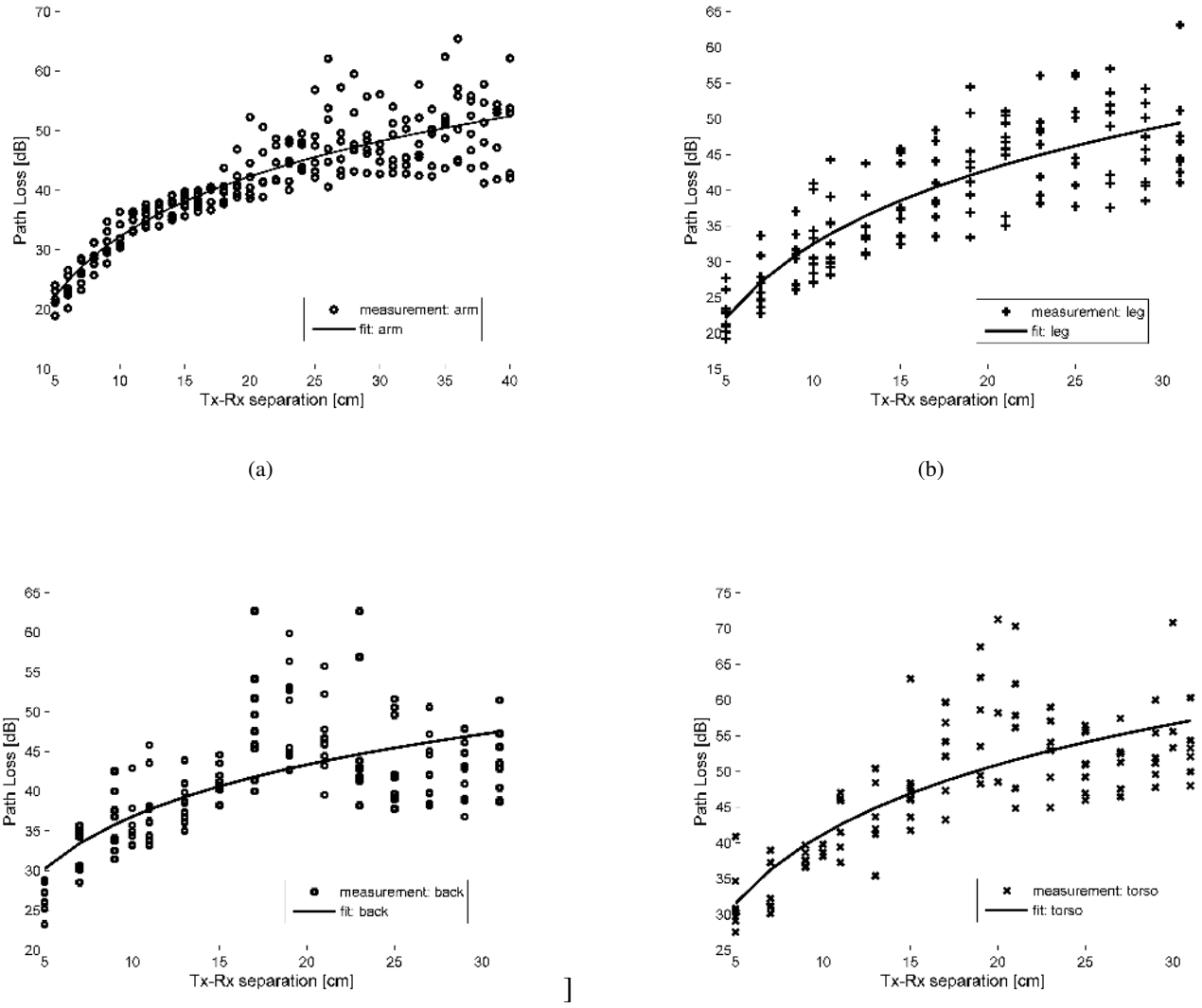

]

Fig. 3. Measured path loss and fitted models versus antenna separation along (a) the arm, (b) the leg, (c) the back, and (d) the torso.

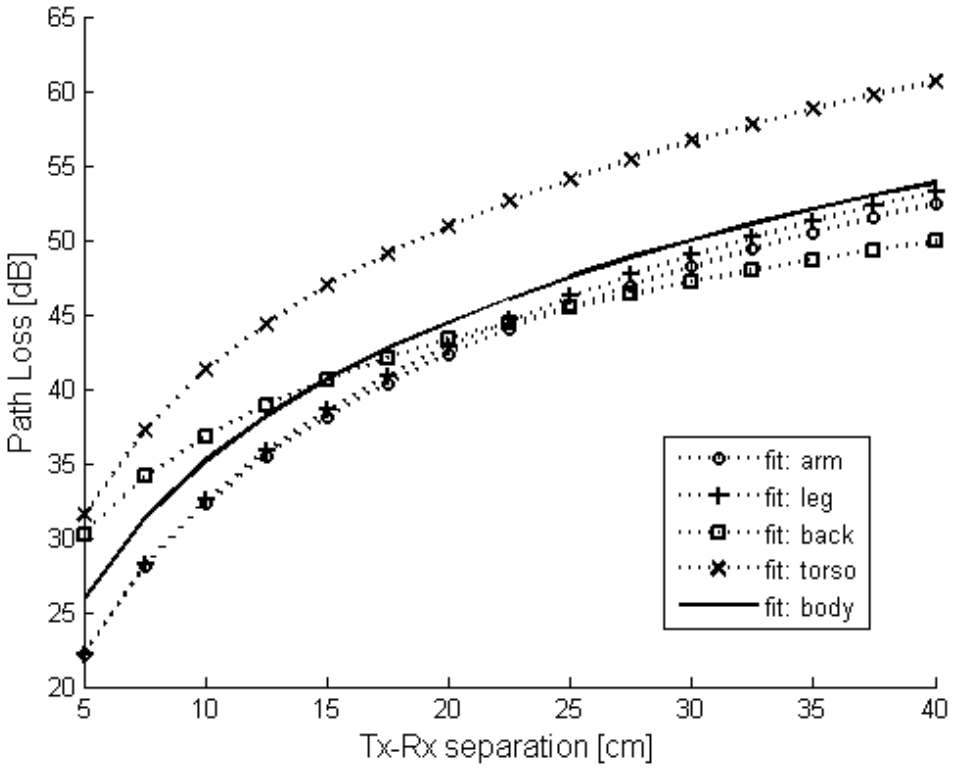

Fig. 4. Path loss models derived from measurements along the arm, torso, back and leg.

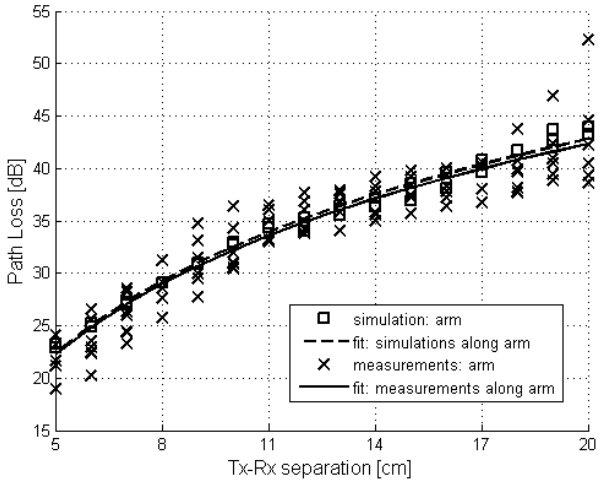

(a)

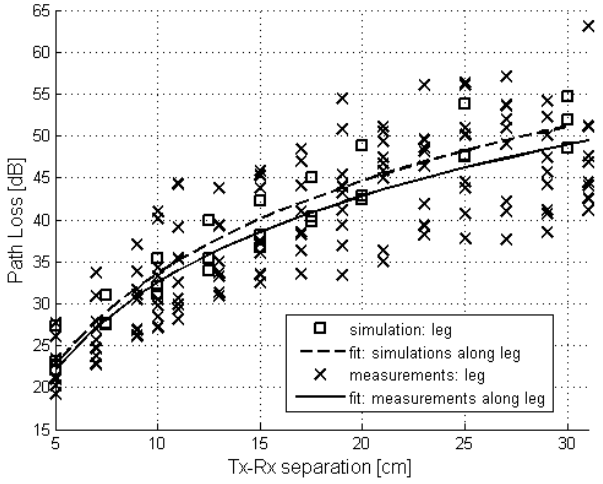

(b)

Fig. 5. Simulated and measured path loss values and fitted models versus antenna separation along (a) the arm and (b) the leg.

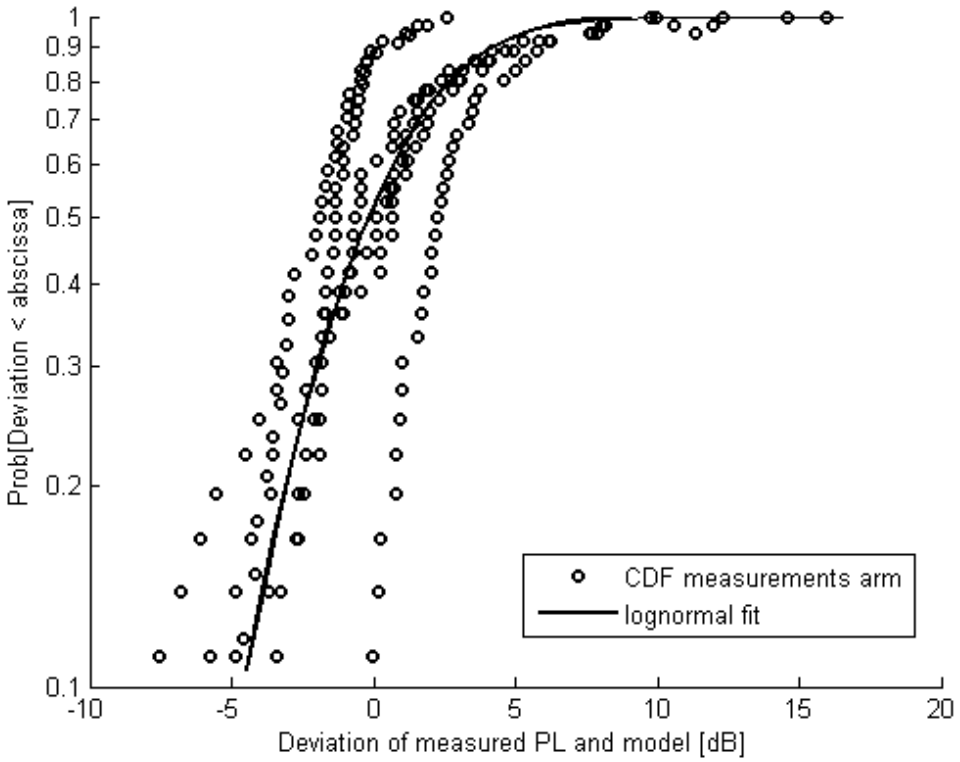

Fig. 6. Cumulative distribution function and lognormal distribution fit of the deviation of the measured path loss and model along the arm.

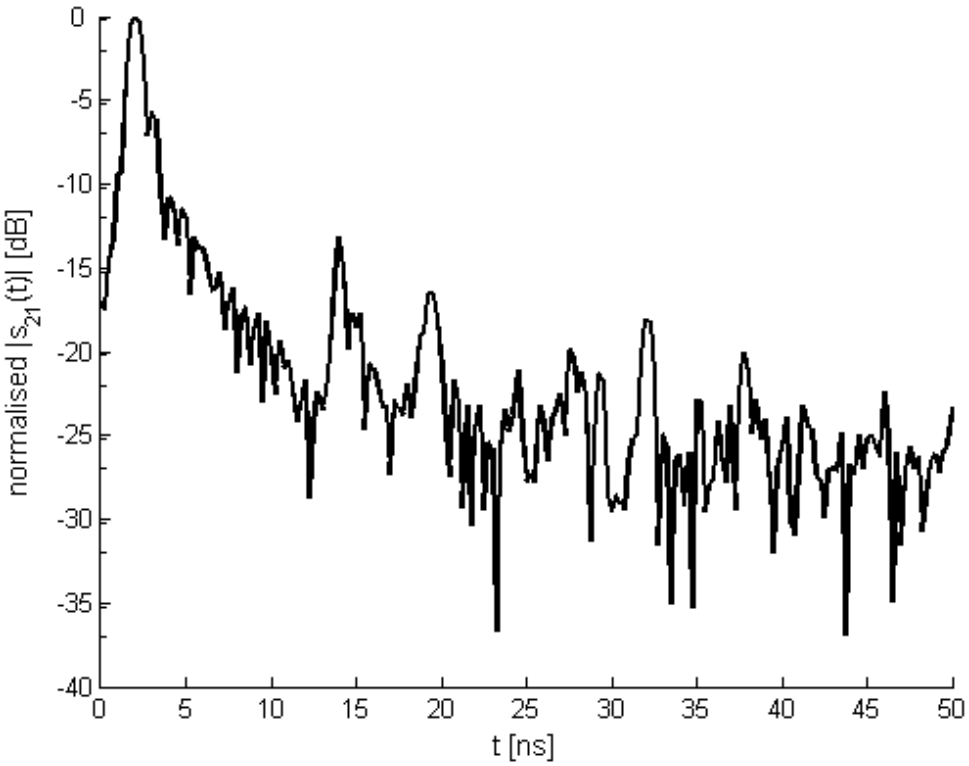

Fig. 7. Measured normalized impulse response along the arm for an antenna separation of 5 cm on a logarithmic scale.

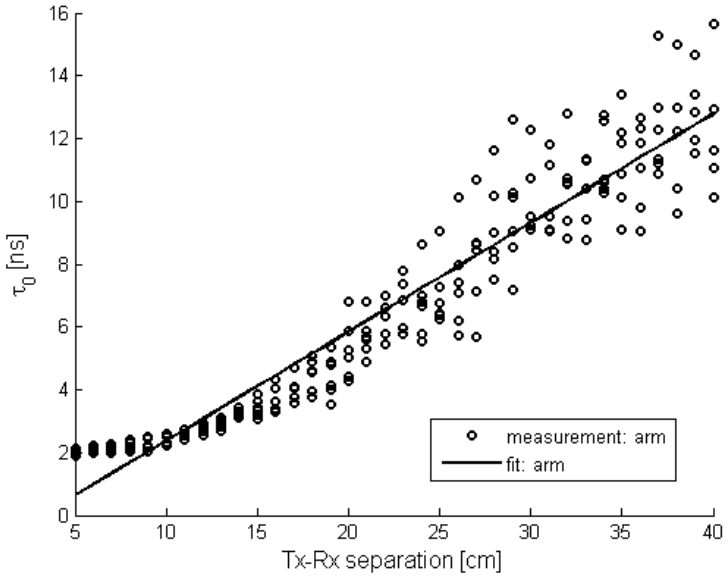

(a)

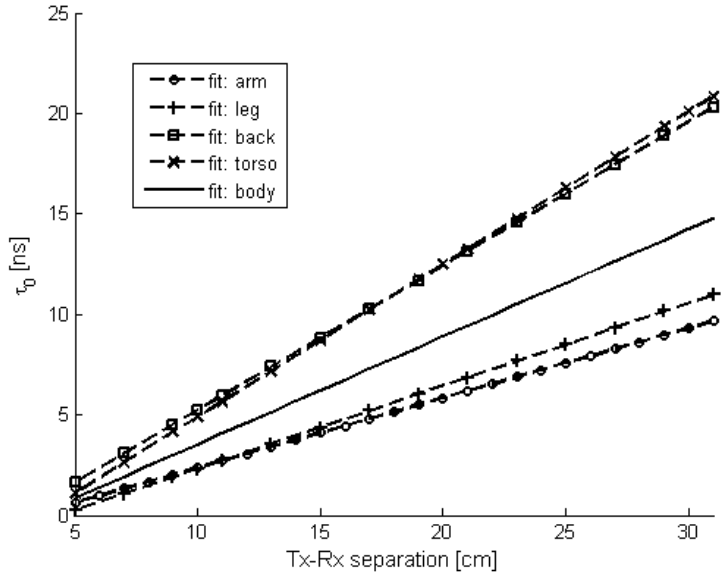

(b)

Fig. 8. Mean excess delay τ_0 versus antenna separation: (a) measurements and linear fit along the arm, and (b) all fitted models.

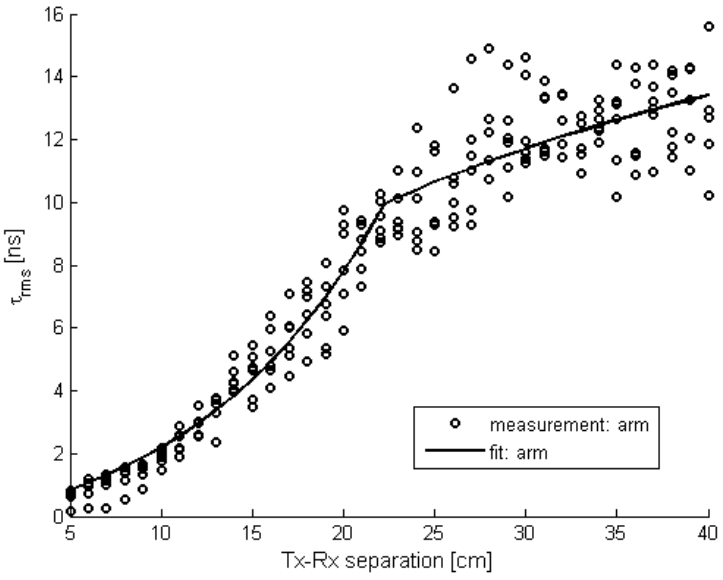

(a)

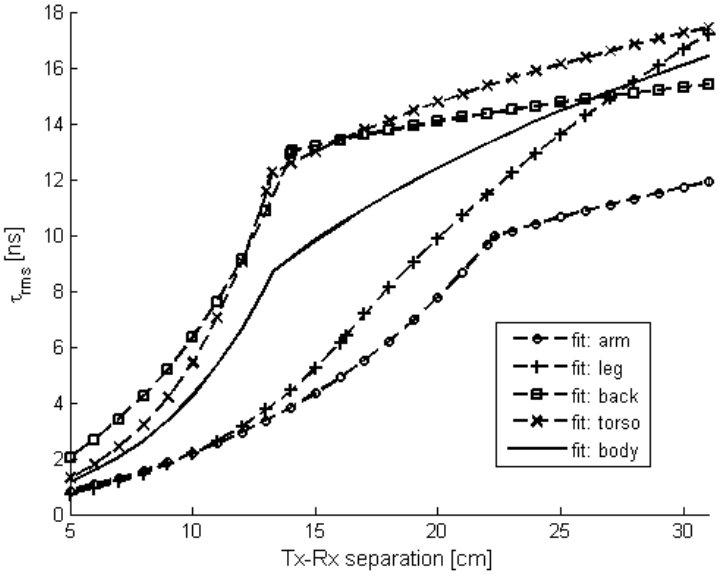

(b)

Fig. 9. RMS delay spread τ_{rms} versus antenna separation: (a) measurements and exponential/logarithmic fit along the arm, and (b) all fitted models.

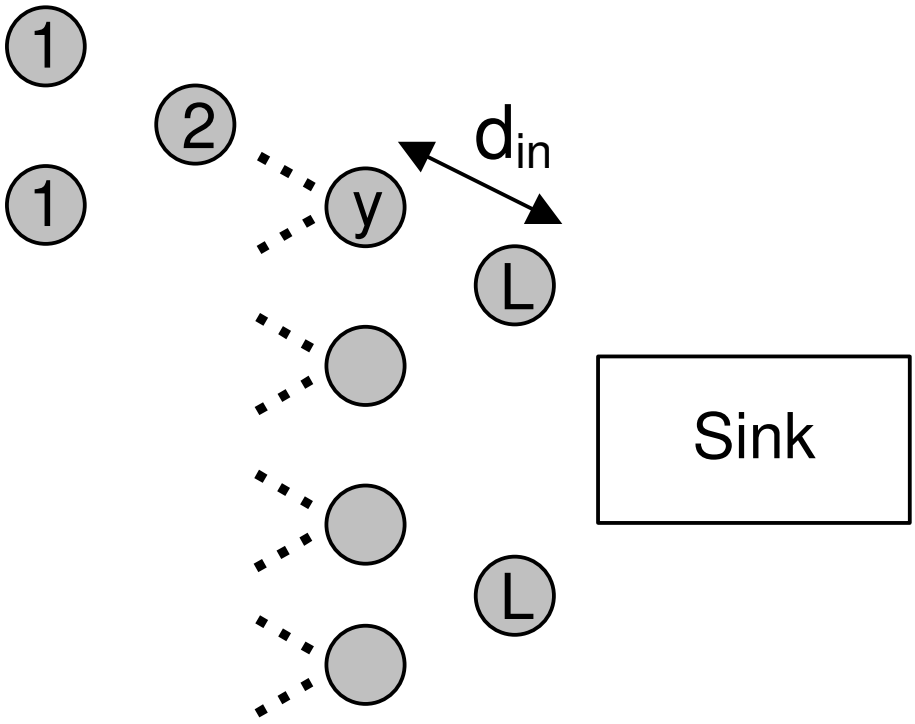

Fig. 10. Full binary tree topology (ζ = 2) with L levels and a fixed inter-node distance d_{in}.

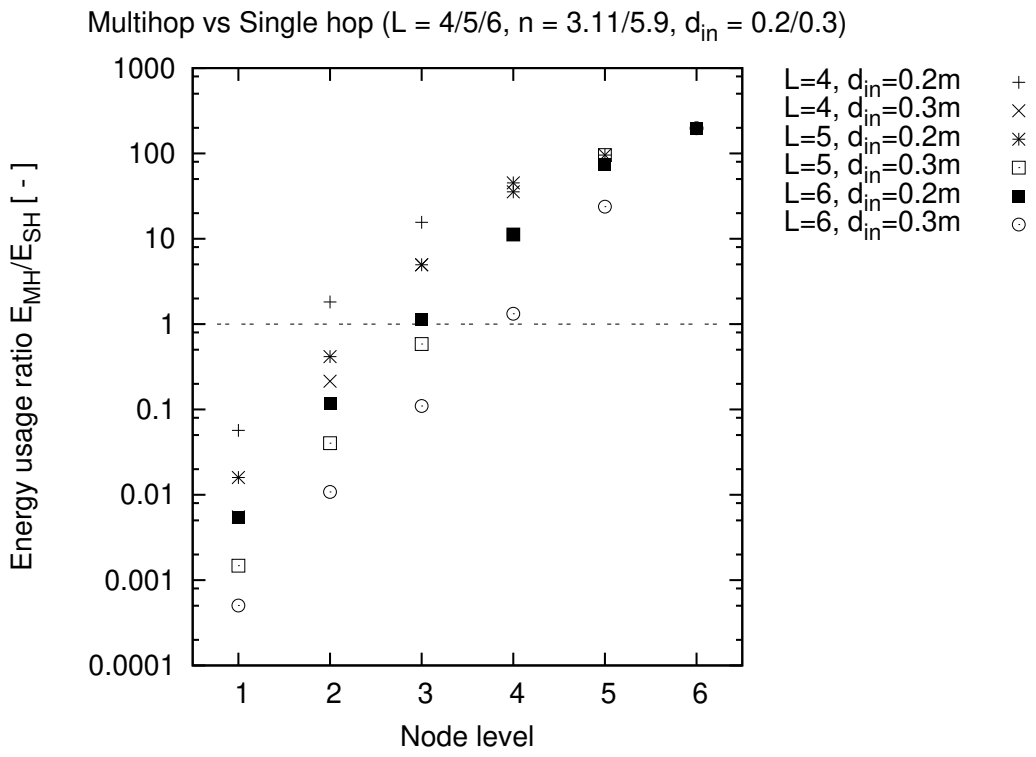

Fig. 11. Energy usage ratio E_{MH}/E_{SH} of multi-hop versus single-hop scenario, in a tree network (ζ = 2) with 4, 5 and 6 levels (L) and inter-node distance d_{in} = 20 cm or 30 cm.

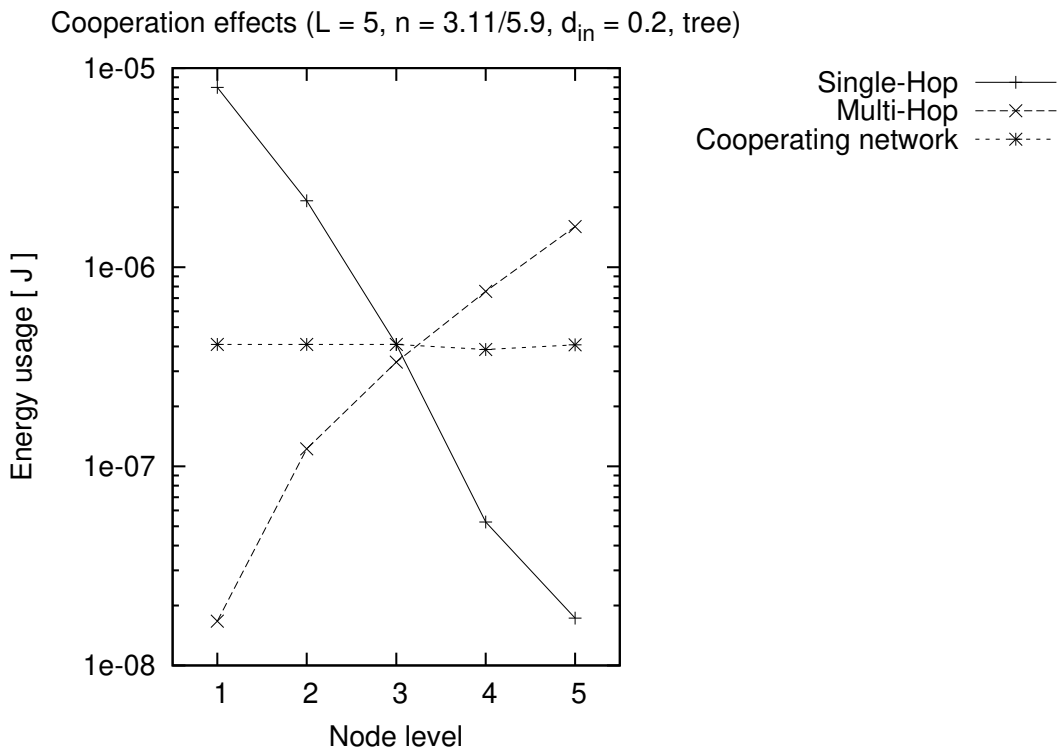

Fig. 12. Energy usage for a tree topology with ζ = 2 and inter-node distance d_{in} = 20 cm: comparison between cooperating, a single-hop scenario and a multi-hop scenario.